DOI: 10.13009/EUCASS2019-1051

Ignition and Flame Propagation Dynamics in a Scramjet Cavity-Based Flame Holder

Stephen D. Hammack and Timothy M. Ombrello***
U.S. Air Force Research Laboratory, Aerospace Systems Directorate
2130 Eighth Street, Wright-Patterson Air Force Base, Ohio, 45433 USA
**stephen.hammack.2@us.af.mil*
***timothy.ombrello.1@us.af.mil*

Abstract
Scramjet ignition is highly dependent upon the location of energy deposition because of the spatial variation of fuel concentration and flow properties. We investigated the spatial dependence of cavity ignition on energy deposition as a function of different fueling configurations. Energy was deposited (~100 mJ) via either laser-induced breakdown or spark plug(s) located throughout a cavity in a Mach 2 flow. Successful ignition was biased towards energy deposition near the rearward facing step of the cavity where fuel concentration and local flow conditions were favorable for ignition kernel survival and flame growth.

1. Introduction

Ignition in recirculating flows of flame holders in supersonic flow is contingent upon having favorable conditions at specific spatial locations and time in order to be successful. At the energy deposition location the reactive mixture needs to be flammable to support the inception of chemical heat release. The local conditions around the ignition kernel then need to be favorable for self-sustained flame propagation, or the kernel needs to be transported to such favorable locations before fluid dynamic strain and heat loss forces extinction. Once significant heat release and flame propagation occurs, the global/bulk recirculation of the flame holder flow needs to be capable of replenishing the reactants and mixing with elevated temperatures and combustion products in order achieve self-sustained steady operation. The multitude of local and global processes therefore necessitates a thorough understanding of the initial conditions and the sensitivities thereof.

Part of the challenge in achieving a unified understanding of the necessary and sufficient conditions for flame holder ignition is a lack of knowledge of the initial fuel distribution. Small variations in global fueling schemes can yield large changes in local fuel concentrations [1]. Therefore, local measurements or distribution of fuel in the flame holder is critical to achieve a firm understanding of ignition [2]. Additionally, when different locations of energy deposition for ignition are used, the situation is exacerbated because of the multiple local and global influences a play [3-5].

The goal of the present work is to assess the sensitivities of the spatial location of energy deposition via a spark discharge towards ignition success. Four locations of a conventional automotive-style spark discharge in the base of a cavity flame holder in a Mach 2 flow were used along with upstream and/or direct cavity fueling. A pulsed Q-switched laser provided a second means of energy deposition, and was used to probe the ignitibility at locations away from cavity surfaces. Measurements of the heat release via kHz visible chemiluminescence imaging were used along with the initial spatial distributions of fuel to better understand the multi-step processes involved from energy deposition to self-sustained steady operation of a cavity flame holder.

2. Experimental Setup

2.1 Flow Tunnel Facility

A generic cavity-based flame holder in the Research Cell 19 continuous flow supersonic tunnel facility at Wright-Patterson Air Force Base was used as the test configuration for the ignition studies. Both the facility [6] and the cavity geometry [3] have been described in detail elsewhere, and therefore only a brief description is provided herein. A full-

DOI: 10.13009/EUCASS2019-1051

span (15.24 cm) cavity was used with a depth of 1.65 cm, length (to the middle of the closeout ramp) of 6.6 cm, and a closeout angle of 22.5° to the cavity floor. The bottom wall of the tunnel, in which the cavity resides, has a divergence of 2.5° in order to reduce choking due to heat release. Four automotive-style non-resistive spark plugs were located in the base of the cavity (see Figure 1).

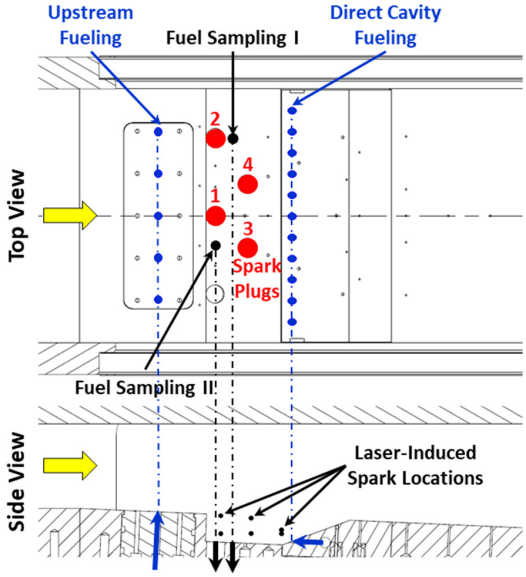

Figure 1: Experimental set-up with fuel injection, spark igniter, and fuel measurement locations.

Two igniters were located against the cavity step, along the streamwise centerline (igniter 1) and 4.7 cm off centerline (igniter 2), and two were located 2.54 cm downstream of the step, 1.9 cm off of each side of the centerline (igniters 3 and 4). Excitation was provided with a commercial transistorized coil system that provided up to 100 mJ per pulse with a spark duration of approximately 2-3 ms. Fuel (C_2H_4) was injected from two locations either separately or simultaneously, and was controlled using calibrated sonic nozzles. Direct cavity injection was achieved using eleven evenly spaced 2.0 mm diameter holes (across the span) in the cavity closeout ramp and upstream injection was achieved using five evenly spaced 2.5 mm diameter holes (across the span) 28.6 mm upstream of cavity step. A flow Mach number of 2, total temperature of 589 K, and total pressure of 483 kPa were used for all experiments.
In addition to the spark plug igniters, ignition was also achieved via laser-induced sparks at locations throughout the cavity away from the wall. The laser spark was generated with a frequency-doubled Nd:YAG laser (New Wave Research, Gemini 200) at 532 nm with 5 ns full width half max (FWHM) pulse width. Energy deposition via the laser pulse was measured using a beam splitter prior to entering the tunnel and was maintained at approximately 100 mJ. The volume of the laser-induced spark plasma was approximately 1 mm^3 [7,8].

2.2 Fuel Concentration and Distribution Measurements

Extractive sampling in the base of the cavity was used to measure the average fuel concentration prior to ignition, and the results were published previously [1]. While the measurements do not describe the fuel distribution in the entire cavity, they do define a means of comparison between ignition tests because of the proximity to the energy deposition locations. Two measurement locations in the base of the cavity were used. Location I was 16.3 mm downstream from the step and 47.2 mm off of the streamwise centerline and location II was 5.6 mm downstream from the step and 17.3 mm off of the streamwise centerline. A heated line was connected to a Nicolet iS50 FTIR with a 2 meter path cell where measurements were taken at a pressure of 20 kPa to ensure rapid and consistent sampling from the cavity. Calibrations were performed with known concentrations of C_2H_4 at the same absorption cell conditions offline.
The distribution of fuel prior to ignition was also measured via infrared (IR) absorption imaging. An extended area blackbody source (CI Systems SR800HT) and infrared camera (FLIR SC6800 camera with a 100 mm focal length StingRay lens using a 3.24 µm centered optical filter [0.1 µm FWHM]) was used. The path-integrated absorption of light from C_2H_4 molecules within the filter band and across the span of the tunnel was used to quantify the average fuel concentration. More details of the set-up can be found in a previous publication [1].

DOI: 10.13009/EUCASS2019-1051

2.3 Heat Release Measurements

The time dependent heat release was qualitatively measured via broadband visible chemiluminescence using a Photron SA-Z CMOS camera. Optical access was achieved through fused quartz windows that comprised the side walls of the cavity. The chemiluminescence was imaged at a downward angled view in order to capture both streamwise and spanwise flame spread within the cavity, at a rate of 40 000 frames per second (fps) when the spark igniters were used and a rate of 50 000 fps during laser-induced ignition.

3. Results and Discussion

3.1 Initial Fueling Conditions

To provide a baseline means of comparison between ignition cases, the initial fuel concentrations prior to ignition were measured for direct cavity and upstream fueling. The two measurement locations were nearly co-located with the spark plug igniter locations, and therefore provided an overall estimate of the conditions present across a broad range of fueling conditions. Figure 2 shows the results of the fuel concentration (and equivalence ratio) as a function of direct cavity and upstream fueling. For direct cavity fueling the variation across the span was minimal, but upstream fueling shows a small spanwise variation for the fueling rates used in the current investigation. It is important to note that with direct cavity injection, the entire lean to rich range is easily attained because of the nearly linear increase in concentration with fueling rate. For upstream fueling there is a fairly linear dependence in concentration with fueling rate up to approximately 350 standard liters per minute (slpm) (standardized to 294 K and 101 kPa), with a leveling off and small decrease with higher fueling rates. The insensitivity of cavity concentration to fueling rates with upstream injection is expected because of being reliant upon entrainment through the shear layer. Therefore, the relative distribution of the fuel plume as it encounters the shear layer will play a critical role in the entrainment dependence. The result is a fuel concentration in the cavity that never exceeds approximately 5% (molar), or an equivalence ratio of approximately 0.75.

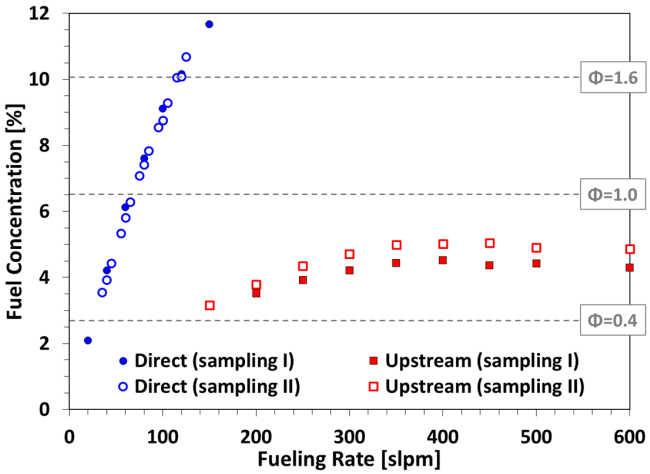

Figure 2: C_2H_4 molar concentration (and equivalence ratio) at two sampling locations in the cavity as a function of direct cavity and upstream fueling rates.

3.2 Ignition with Direct Cavity Fueling

The ignition limits of the cavity with direct fueling were initially assessed using spark igniters 3 and 4 and discretely increasing (or decreasing) the fueling rate to find the lean (or rich) limits. For the test at each fueling condition both spark igniters were triggering simultaneously 20 times at 50 Hz. Steps of several liters per minute were used and the lean and rich limits were found to be 42 and 105 slpm, respectively. Note that while 105 slpm is the rich ignition limit for the cavity using these spark igniters, the rich blowout limit is at a significantly higher fueling rate (>200 slpm). Alternatively, the lean ignition limit is near the lean blowout limit (~35 slpm).

DOI: 10.13009/EUCASS2019-1051

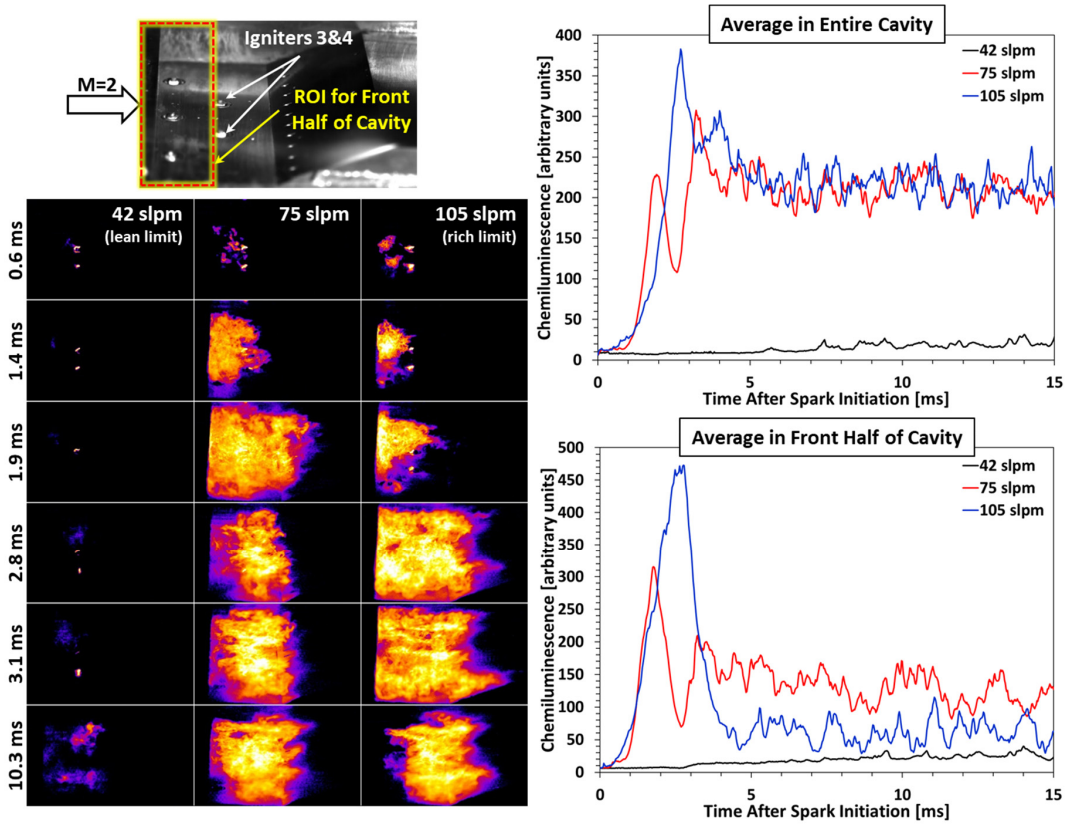

Figure 3: Still images and plot of time dependent chemiluminescence for direct cavity fueling cases at lean, near stoichiometric, and rich ignition limits. Note that the images were flipped horizontally to show flow from left to right.

The ignition process was then imaged at the lean and rich ignition limits, as well as near stoichiometric (75 slpm) and the results are shown in Figure 3. The time sequence of the chemiluminescence clearly shows the different time scales involved in ignition, with the near stoichiometric (75 slpm) case showing rapid flame spread at early times, with the rich limit (105 slpm) being slightly slower, but still much faster that the lean limit case (42 slpm). To better visualize and quantify the ignition process, the average visible chemiluminescence can be used as a marker of the heat release or burning flux since the emission comes primarily from excited species CH* and C_2* that are only present in the flame front [9]. The top right plot in Figure 3 shows the average chemiluminescence intensity for the entire image for each fueling case as a function of time. For the 75 slpm case, there was a rapid increase in heat release, but then a significant decrease before rising to the peak overall heat release rate. The 105 slpm case shows the same peaking of heat release before decreasing to the steady state cavity burning levels. The spike of heat release can be tied to the spatial dependence of heat release during the initial flame spread. To emphasize this point, the heat release in a region of interest (ROI) in the front portion of the cavity, as shown in the top image of Figure 3, is shown in the bottom plot of Figure 3. The contribution of the overall heat release was predominately coming from the front portion of the cavity near the step. Referring to the 75 slpm images as an example in Figure 3, the kernels from the spark igniters are first shed and were advected towards the step where a low velocity region was present within the first millisecond after the spark discharge was initiated. The flame rapidly spread across the span by 1.4 ms, and was pulled into the shear layer and downstream by 1.9 ms. The rapid development of the flame across the span of the cavity occurred on a time scale that was shorter than the bulk recirculation time (~1.5 ms), which allowed for the sharp increase in heat release before significant exchange with the freestream could occur. The heat release then decreased near the step of the cavity and the heat advected downstream by the shear layer was recirculated over the closeout ramp to ignite the fuel plumes by 2.8 ms. The final result was a mix of burning in the wake of the ramp injectors, as well as in the shear layer. The rich limit case (105 slpm) followed a similar trend with a slightly different final flame stabilization that was more concentrated over the closeout ramp. The lean limit case (42 slpm) had a very slow ignition process where burning remained contained in the cavity, below the shear layer, with minimal heat release throughout. Overall, all three baseline cases with direct cavity fueling emphasize the importance of the kernel advection towards the cavity step and rapid spanwise flame spread on the order of the bulk recirculation time that leads to a spike in heat release during the

DOI: 10.13009/EUCASS2019-1051

ignition process. Additionally, the fuel concentrations at the lean and rich ignition limits were approximately 4.4 and 9.3 % (molar), which is approximately an equivalence ratio of 0.75 and 1.47, respectively.

3.3 Ignition Dependence on Energy Deposition Location

With the baseline set of ignition conditions showing the key features of the processes involved, the spatial dependence of the spark discharge location was investigated. At a fixed fueling rate of 105 slpm, which is near the rich ignition limit, four different spark igniter configurations were tested. Igniters 1, 2, and 4 were tested individually, as well as all igniters (1,2,3,4) simultaneously. Cavity ignition was successful for all locations and the images of the processes are shown in Figure 4 along with a plot of the heat release in the front half of the cavity as a function of time. Beginning with igniter 4, the process was similar to what was shown in Figure 3 when both igniters 3 and 4 were used simultaneously. Ignition kernels were shed from the spark discharge and were advected towards the step of the cavity. Spanwise flame spread then transpired, resulting in a spike in heat release as shown in the right plot of Figure 4. The results of igniter 4 showed a similar time scale for the ignition process even though the kernels did not have to advect towards the step of the cavity. Rather, the flame had to grow across most of the span of the cavity, such as between 2.1 and 3.5 ms, which resulted in approximately the same time scale for ignition. The ignition process with igniter 1 was much more rapid. Within 0.8 ms there was a large ignition kernel present, and by 1.5 ms the flame had already spread across half the span of the cavity. Because of this early heat release, the ignition process was nearly complete and steady-state cavity burning achieved by 3.5 ms, which was the middle of the propagation process in the front half of the cavity for igniters 2 and 4. When all four igniters (1,2,3,4) were used simultaneously, while the ignition process was the fastest, it was only marginally faster and had the same propagation process as with igniter 1. The result indicates that igniter 1 appears to be the most optimal of the four locations tested when only a single igniter was used. The success appears to be driven by two factors. First, there was near immediate production of an ignition kernel from the discharge (within several hundred microseconds of discharge initiation), and second, there was rapid flame propagation in the front half/near the step of the cavity that occurred on a time scale that was shorter than the bulk recirculation time. Both factors can be attributed to the favorable conditions present near the rearward facing step of the cavity where the fuel concentrations are rich with little fluctuations, and the flow velocity is low. Therefore, ignition kernels can incubate and the flame can grow rapidly before influence by the bulk recirculating flow.

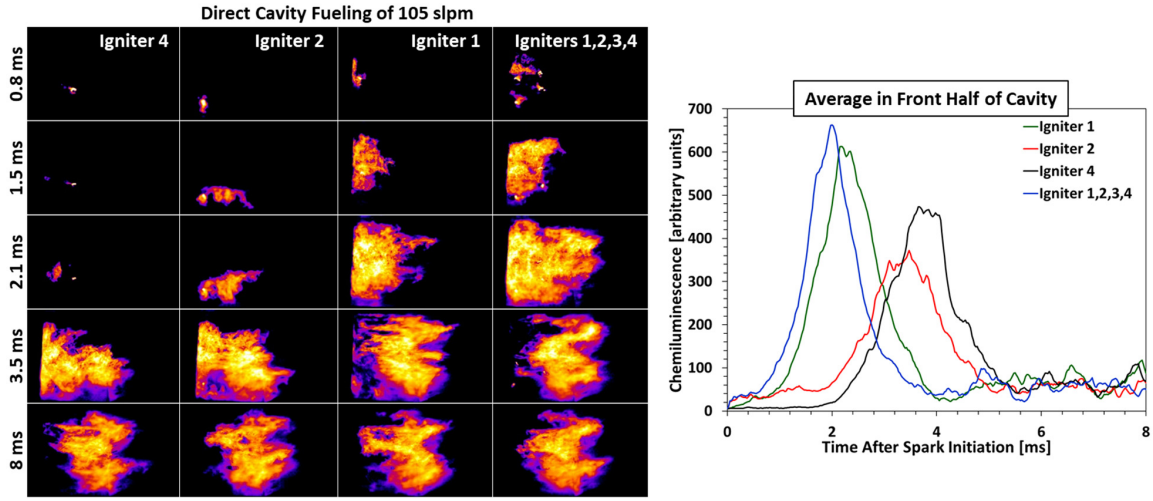

Figure 4: Still images and plot of time dependent chemiluminescence for direct cavity fueling cases near the rich ignition limit. Note that the images were flipped horizontally to show flow from left to right.

Moving beyond the energy deposition locations along the floor of the cavity from the spark plugs, laser-induced spark ignition was performed. A laser-induced spark could be located throughout the volume of the cavity, and six specific locations were chosen along the streamwise centerline. The laser-induced spark locations A and B were positioned streamwise similarly to the near-step (1 and 2) and mid-cavity (3 and 4) spark plug igniters, respectively, whereas location C was closer to the cavity close-out ramp. Locations D, E, and F were along the bottom portion of the shear layer where ignition was still possible at the specific streamwise locations. Figure 5 shows images of the ignition process for laser-induced ignition locations of A, B, and C along with a plot of the average chemiluminescence signal level for a direct cavity fueling rate of 55 slpm (near the lean ignition limit). The entire image chemiluminescence signal was used because the change of laser ignition location was accompanied by a change in camera position; the

DOI: 10.13009/EUCASS2019-1051

laser and camera were mounted to the same translation table. This resulted in an imaging perspective unique for each location and no practical method of obtaining a region-of-interest consistent across the data was possible.

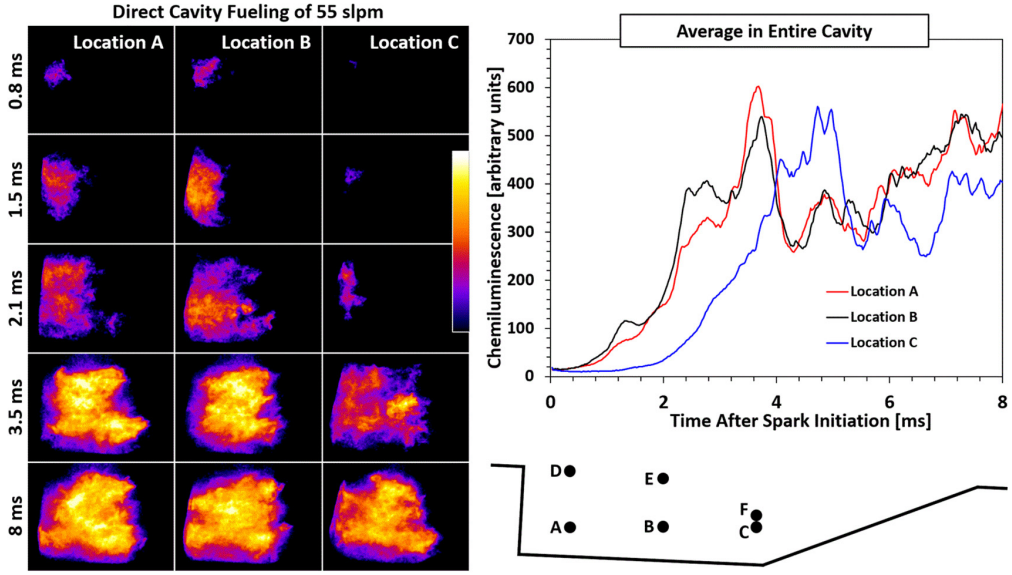

Figure 5: Still images and plot of time dependent chemiluminescence for direct cavity fueling near the lean ignition limit. Laser breakdown was used as the energy deposition source. Note that the images were flipped horizontally to show flow from left to right.

The chemiluminescence images for locations A and B illustrate the same behavior observed with the spark igniters, and in both cases the flame spread rapidly along the step portion of the cavity by approximately 2.1 ms while location C significantly lagged behind. The difference in ignition progress was also evident in the plot where locations A and B reached a maximum signal approximately 1 ms faster than the location C. The cause of the difference in the ignition progression rates was investigated by examining flame kernel advection and propagation immediately after the laser-induced spark. Contours at four instances in time after the laser-induced spark were superimposed on a time lapse image at each of the six laser-induced spark locations and are presented in Figure 6. Location A, which was located near the cavity step region, showed very little advection of the kernel, with flame growth radially within the first 625 µs. Location B showed similar growth rates, but after advection of the ignition kernel towards the cavity step region within the initial 225 µs. The advection of the ignition kernel was more profound for location C where nearly 0.5 ms was required for the kernel to traverse the cavity from the ramp to step region before flame growth could ensue.

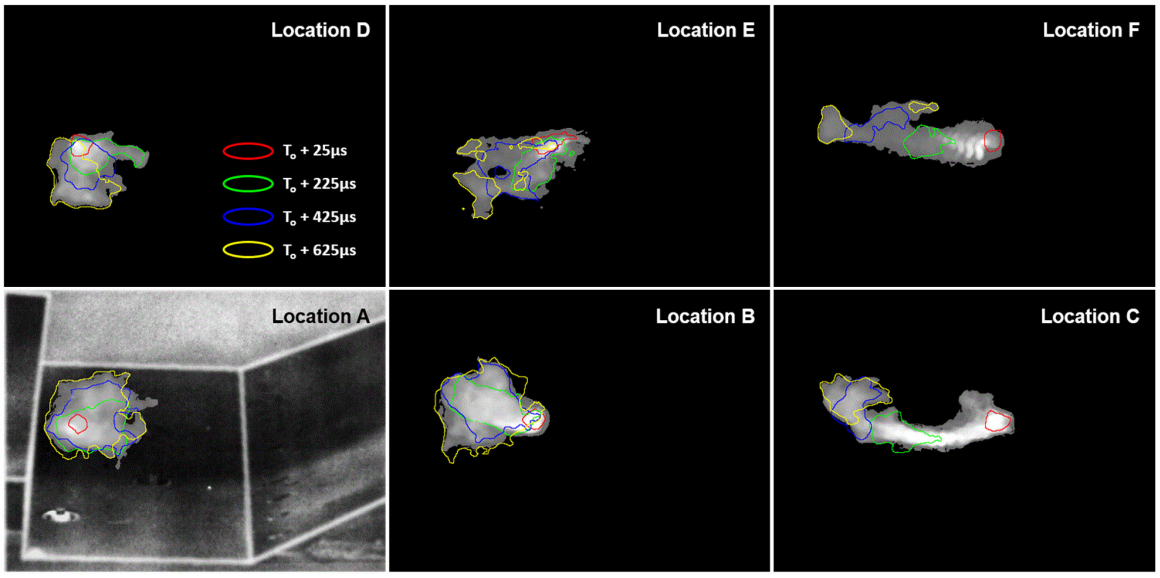

DOI: 10.13009/EUCASS2019-1051

Figure 6: Contours at four instances in time after the laser-induced spark superimposed on a time lapse image at each of the six locations.

The different paths of the ignition kernel and when flame propagation ensued is attributed partly to the flowfield relative to the laser-induced spark locations. Figure 7 shows the average contours of the velocity field as well as select average streamlines in the cavity. Moving from location A to C results in an increase in the magnitude of local flow velocity, from less than 25 m/s to nearly 100 m/s. Location A showed very little ignition kernel movement prior to flame spread since the local flow velocity was lower that the flame propagation rate. For location B, the local flow velocity initially dominated and the kernel moved towards the cavity step, but since the gradient in the local flow velocity was deceasing, flame propagation rapidly started to dominate. For location C the local flow velocity dominated the initial times with advection of the kernel to the lower velocity region near the cavity step region before flame propagation.

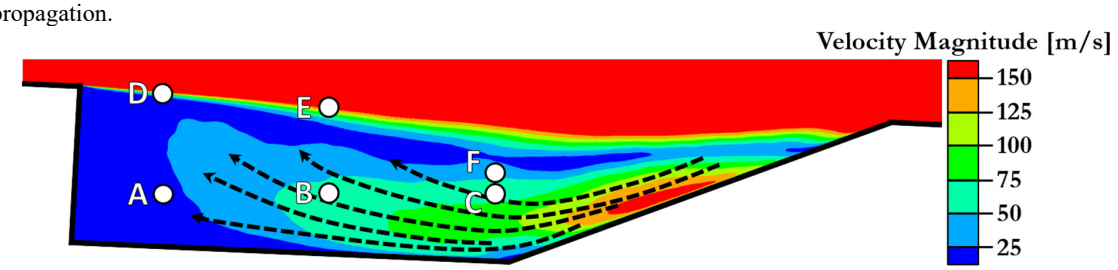

Figure 7: Average fluid motion results from simulations of the cavity prior to burning.

While advection of the kernel to a lower velocity region was critical to allow for flame propagation to dominate, the local fuel concentration was also important. Figure 7 shows the locations for the laser-induced spark relative to average fuel concentration distributions across the span of the cavity from IR absorption measurements. Similar to the gradients in velocity, there were gradients in the concentration where more favorable (closer to stoichiometric) conditions were present at locations closer to the cavity step region. Therefore, the advection of the kernels from locations 2 and 3 towards the step region provided lower velocity and closer to stoichiometric fuel concentrations for rapid flame propagation.

Laser-induced spark ignition locations D, E, and F further emphasize the competition between local flow velocity, fuel concentration, and flame propagation. In Figure 6, location D showed that there was little kernel advection before flame propagation towards the floor of the cavity step region. Interestingly, since location D was at the edge of the shear layer, there was a stretching of the kernel at early times between 25 and 225 µs where the kernel was elongated in the streamwise direction. Nevertheless, a portion of the kernel was in the low velocity region below the shear layer where flame propagation could dominate. Location E followed a similar trend, but there was increased influence from the high velocity in the shear layer. At the first instance in time at 25 µs, the ignition kernel was elongated in the streamwise direction because of the flow. The ignition kernel was stretched and shredded, but not enough to completely extinguish. While the average local flow velocity advected the kernel towards the cavity ramp, there were multiple portions of the kernel that began to propagate into a flame. The flame propagation continued to compete with the local flow velocity, but continued to move to more favorable fuel concentrations near the cavity step region. The result was a successful cavity ignition event, but after a significantly long period of time because the bulk recirculating flowfield of the cavity recirculated the flame before it could reach the cavity step region for eventual rapid flame propagation. The ignition process at location F in Figure 6 had features of both locations C and E where the local flow velocity initially dominated to advect the kernel towards the cavity floor and cavity step region, but through an unfavorable set of flow and concentration conditions near the ramp and fuel injection plumes.

DOI: 10.13009/EUCASS2019-1051

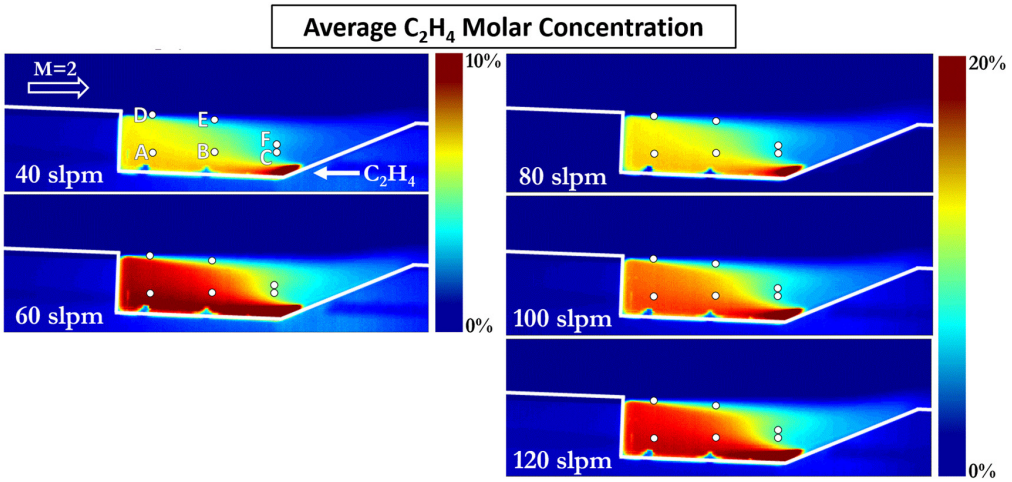

Figure 8: Average fuel concentration distribution across the span of the cavity as measured by IR absorption imaging. Note the difference in scaling of the colormap between the left and right columns.

The competing processes involved in the ignition process across the six laser-induced spark ignition locations is illustrated by the number of ignition attempts required across a range of direct cavity fueling rates shown in Table 1. Failed ignition series are noted using a 0/(number of pulses in series) notation. While the results are not statistically rigorous, they emphasize the trends where energy deposition near the cavity step region and along the floor have the broadest range of ignitable fueling rates, and hence fuel concentration conditions.

Table 1: Successful ignition attempts for six laser-induced spark locations as a function of direct cavity fueling rates.

	A	B	C	D	E	F
45	2	17	100	0/200	0/200	
55	1	1	1, 3, 0/20	14, 0/20	0/20, 81	124, 85
75	1	1	1	1	3	78
95	1	1	11	1	4	6
115	1	5	2	4	23	3
135	74	0/20, 111	0/200	0/200	0/200	0/50

Figure 9 presents a portion of the data in Table 1 in a diagram to emphasize the effect of location on the range of ignitable cavity fueling rates. A colored stripe indicates an ignitable location for the flow rate associated with that color. For this purpose, a location is deemed ignitable if less than 12 laser pulses were required for ignition *and* there were no instances of a failed series of laser pulses. This is somewhat arbitrary but the general trend is not dependent on the exact selection criteria.

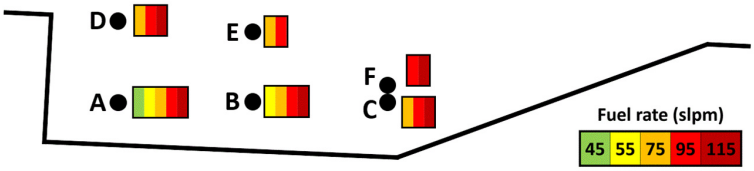

Figure 9: Ignitable cavity fuel rates at each of the six locations for laser breakdown. See accompanying Table 1.

DOI: 10.13009/EUCASS2019-1051

3.4 Ignition with Upstream Fueling

Moving beyond direct cavity fueling, ignition was also tested with the spark plug igniters at the four locations (1-4) for multiple upstream fueling cases. Specifically, an upstream fueling rate of 400 slpm was used since it was near the maximum fuel concentration achievable without direct cavity fueling, which was approximately 4.5-5% (molar) as shown in Figure 2. The fuel concentration was near the lean ignition limit with direct cavity fueling, which was approximately 4.4% (molar). The spark discharge was fired 20 times at 50 Hz for each individual location, and ignition was only possible when igniter 1 was used. The results follow what was found for the direct cavity fueling cases where the igniter 1 location showed the fastest and most robust ignition process when a single location was used.
When a small quantity of fuel was injected into the cavity, ignition was more successful since the equivalence ratio was closer to stoichiometric. For example, with upstream fueling of 450 slpm using igniters 3 and 4 with 20 pulses at 50 Hz, ignition was not possible. When 20 slpm of fuel was injected into the cavity in addition to the 450 slpm upstream and using igniters 3 and 4, ignition occurred consistently on the first pulse. The difference between the two cases is not surprising since 450 slpm upstream fueling produces conditions in the cavity that is near the lean ignition limit, whereas the combined 450/20 slpm upstream/direct cavity would result in near stoichiometric conditions because of the additive process of ~4.8% and ~2% fuel concentration when referring back to Figure 2. Note that previous work showed that the upstream and direct cavity fueling is approximately additive [1].

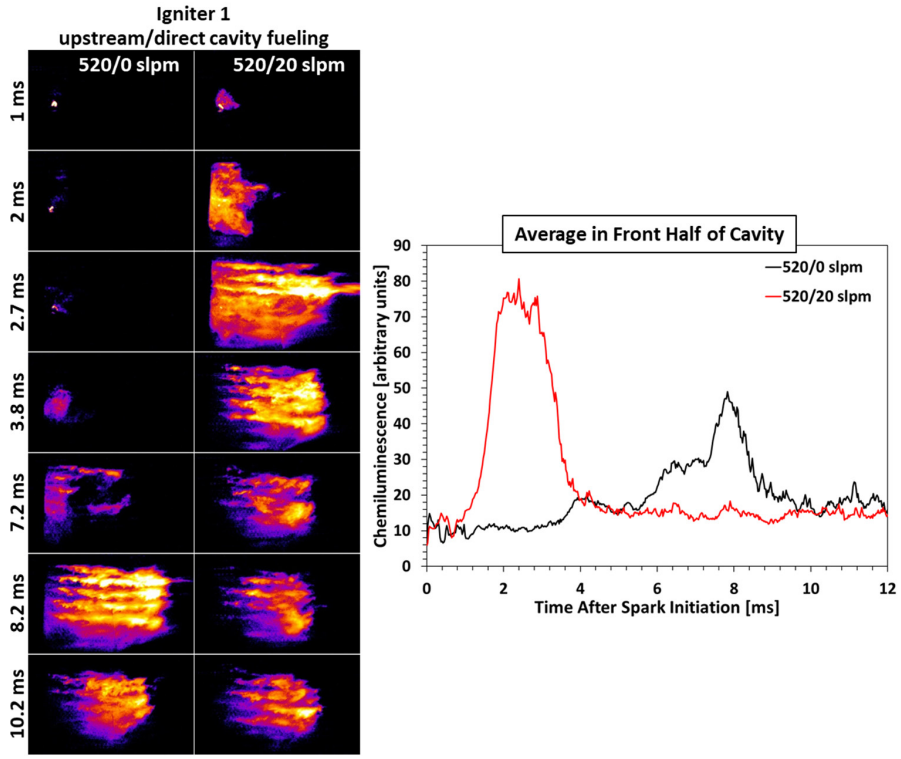

Figure 10: Still images and plot of time dependent chemiluminescence for upstream fueling cases. Note that the images were flipped horizontally to show flow from left to right.

To illustrate the ignition process differences between upstream fueling and upstream/direct cavity fueling, the heat release was imaged via chemiluminescence. A case was chosen where ignition was successful for both fuel injection strategies, and igniter 1 was used. The results are shown in the images and plot in Figure 10. There is a stark difference between the heat release rates at early times between the two fueling cases. For the 520/20 slpm upstream/direct cavity fueling case, there is rapid ignition kernel and flame propagation occurring within 1 ms, whereas the 520/0 slpm case required nearly 3.8 ms to reach the same level of burning. The main difference can be attributed to the rapid flame propagation near the step of the cavity. For the 520/20 slpm case, the process was rapid flame propagation across the span of the cavity near the step, which fed the flame and hot products into the early portion of the shear layer to ignite the fuel plumes from upstream injection. The burning plumes then cycled back elevated temperature and combustion products into the cavity through the shear layer near the closeout ramp. For the 520/0 slpm case, the flame propagation across the span was significantly suppressed, as evident in the chemiluminescence plot between 3.5 and 7 ms. It was not until there was enough heat release near the front step of the cavity that sufficient heat was available at the shear

DOI: 10.13009/EUCASS2019-1051

layer to ignite the fuel plumes from upstream injection. It is important to consider that the cavity had recirculated multiple times during this "run-up" time to achieving steady cavity burning. Therefore, having a favorable set of conditions for flame propagation across the span of the cavity near the step was critical to rapid and successful cavity ignition.

While having an overall distribution of fuel in the cavity that was favorable for burning was important, it appeared to be critical for the fuel distribution to be favorable near the step when ignition was considered. To emphasize this point, the average fuel distribution across the span of the cavity is shown in the IR absorption images in Figure 11. The IR absorption images show the relative distribution of fuel throughout the cavity for direct cavity fueling, upstream fueling, and upstream/direct fueling. For direct cavity fueling in Figure 11(a), the majority of the cavity is deficient of fuel because of the large quantity of dilution air that enters through the shear layer. Therefore, the fuel is distributed fairly uniformly along the floor and near the step. For the upstream fueling case in Figure 11(b), the cavity had a very uniform quantity of fuel throughout the entire volume. While both Figures 11(a) and (b) have approximately the same fuel distribution near the igniter, they did not have the same ignitability. Figure 11(a) was near the lean ignition limit for direct cavity fueling (approximately 42 slpm) and was successfully ignited with any of the four igniters individually. On the other hand, Figure 11(b) had a similar fuel distribution near the igniter, but typically required multiple spark discharge attempts when using any igniter, with a bias of more successful ignition with igniter 1. Therefore, direct cavity fueling appeared to reduce fuel concentration fluctuations that would suppress ignition success. By adding a small quantity of fuel directly to the cavity, as is shown in Figure 11(c), the average fuel concentration increased preferentially in the cavity floor and near the step. Figures 11(b) and (c) are comparable to the fueling schemes shown in Figure 10 where the addition of direct cavity fueling resulted in more rapid spanwise flame propagation near the step. Therefore, having a bias to more favorable (stoichiometric or rich) conditions along the floor and near the step of the cavity was vital for robust ignition success.

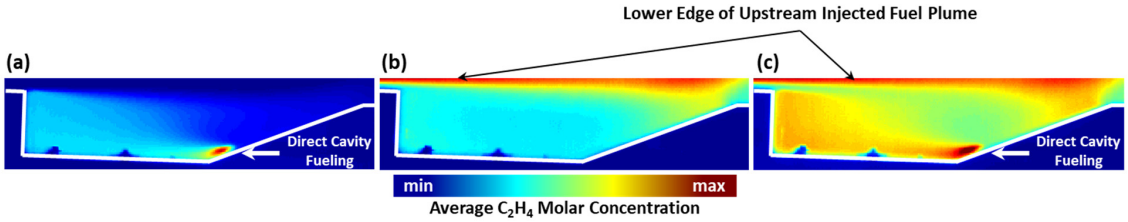

Figure 11: IR absorption images showing the approximate average distribution of fuel for (a) direct cavity fueling, (b) upstream fueling, and (c) upstream/direct cavity fueling. The upstream fueling rate was the same for (b) and (c).

4. Summary and Conclusions

The sensitivity of ignition to the spatial distribution of fuel and energy deposition location was assessed with upstream and direct cavity fueling in a generic cavity-based flame holder in supersonic flow. Qualitative measurements of the heat release was achieved via 40 000 and 50 000 frames per second visible broadband chemiluminescence. The results showed the spatial extent of heat release as a function of time throughout the ignition process. Igniter locations near the cavity step resulted in near immediate ignition kernel development and rapid achievement of self-sustained flame propagation in the cavity. Igniter locations away from the cavity step region were in a competition between local flow velocity, fuel concentration, and flame propagation rates to survive. Ignition kernels in higher velocity regions along the floor of the cavity towards the closeout ramp were rapidly advected towards the cavity step region before flame propagation could ensue. The suppression of flame growth resulted in less ignition success across a range of fueling rates. The fastest and robust ignition events for all fueling cases showed rapid spanwise flame propagation near the cavity step. The flame propagation on time scales shorter than the bulk recirculation time of the cavity allowed for a spike in heat release. Measurements of the pre-ignited fuel concentration via extractive sampling showed that the ignitable range of the cavity was with fuel concentrations of approximately 4.4-9.3% (Φ= 0.75 to 1.47). Furthermore, measurements of the overall fuel distribution via IR absorption imaging showed that having favorable fueling conditions along the floor of the cavity and near the step were critical for robust and successful ignition.

Acknowledgements

The authors wish to thank Dr. David Peterson for supplying simulation results for use in the figures and Mr. N. Sebastian Okhovat and Dr. Michael Rhoby for their assistance with the FTIR and IR imaging experiments. The authors also wish to thank Dr. Seong-kyun Im, Ms. Lydia Wermer, and Mr. Brendan McGann for their assistance and equipment used for laser-induced ignition.

DOI: 10.13009/EUCASS2019-1051

References

[1] T. Ombrello, N.S. Okhovat, M.R. Rhoby, 2018. Measurements of Scramjet Fueling Conditions, *AIAA SciTech, 57th Aerospace Sciences Meeting.* AIAA 2018–1360.

[2] T. Ombrello, E. Hassan, C. Carter, B. McGann, T. Lee, H. Do, D. Peterson, P. Ivancic, and E. Luke. 2016. Establishing the Controlling Parameters of Ignition in High-Speed Flow. *AIAA SciTech 2016, 54th Aerospace Sciences Meeting.* AIAA–2016–0658

[3] T. Ombrello, C. Carter, C.-J. Tam, and K.-Y. Hsu. 2015. Cavity Ignition in Supersonic Flow by Spark Discharge and Pulse Detonation. *Proceedings of the Combustion Institute.* 35:2101–2108.

[4] Zun Cai, Jiajian Zhu, Mingbo Sun, Zhenguo Wang and Xue-Song Bai. 2018. Laser-Induced Plasma Ignition in a Cavity-Based Scramjet Combustor. *AIAA Journal.* 56(12):4884–4892.

[5] Bin An, Zhenguo Wang, Leichao Yang, Xipeng Li, Jiajian Zhu. 2017. Experimental Investigation on the Impacts of Ignition Energy and Position on Ignition Processes in Supersonic Flows by Laser Induced Plasma. *Acta Astronautica.* 137:444–449.

[6] M.R. Gruber, and A.S. Nejad. 1995. New Supersonic Combustion Research Facility. *Journal of Propulsion and Power*. 11:1080–1083.

[7] N.G. Glumac, G.S. Elliott, and M. Boguszko. Temporal and Spatial Evolution of a Laser Spark in Air. *AIAA Journal*. 43(9):1984–1994. doi:10.2514/1.14886

[8] L. Wermer, J.K. Lefkowitz, T. Ombrello, M.S. Bak, and S.-K. Im. 2018. Spatiotemporal Evolution of the Plasma from Dual-Pulsed Laser-Induced Breakdown in an Atmospheric Air. *Plasma Sources Science and Technology*. 27(1). doi:10.1088/1361-6595/aa9fe2

[9] T. Ombrello, D. Blunck, and M. Resor. 2016. Quantified Infrared Imaging of Ignition and Combustion in a Supersonic Flow. *Experiments in Fluids.* 57(9):1–12.